Extending the spectral range of CdSe/ZnSe quantum wells by strain engineering

A. Finke,[1] M. Ruth,[1] S. Scholz,[2] A. Ludwig,[2] A. D. Wieck,[2] D. Reuter,[1] and A. Pawlis[1,*]
[1]*University of Paderborn, Warburger Strasse 100, D-33098 Paderborn, Germany*
[2]*Ruhr-University Bochum, Universitätsstrasse 150, D-44780 Bochum, Germany*
(Received 15 October 2014; revised manuscript received 15 December 2014; published 12 January 2015)

We demonstrate efficient room-temperature photoluminescence and spectral tuning of epitaxially grown ZnSe/CdSe quantum well structures almost over the whole visible spectrum (470–600 nm wavelength). The key element to achieve the observed high quantum efficiency and enormous tuning range was the implementation of a special strain engineering technique, which allows us to suppress substantial lattice relaxation of CdSe on ZnSe. Previous studies indicated that a CdSe coverage exceeding 3 ML on ZnSe results in the formation of extensive lattice defects and complete quenching of the photoluminescence at low and room temperature. In contrast, our approach of strain engineering enables the deposition of planar CdSe quantum wells with a thickness ranging from 1 to 6 ML with excellent optical properties. We attribute the observed experimental features to a controllable strain compensation effect that is present in an alternating system of tensile and compressively strained epitaxial layers and supported this model by calculations of the transition energies of the ZnSe/CdSe quantum wells.

DOI: 10.1103/PhysRevB.91.035409 PACS number(s): 85.60.−q, 71.20.Mq, 78.55.−m, 78.67.−n

I. INTRODUCTION

The wide-gap II-VI semiconductors CdSe, ZnSe, Zn(S,Se), and (Zn,Mg)Se have been extensively investigated in the past decades for possible optoelectronic applications in the blue and green spectral range [1,2]. Light emitting diodes [3,4] as well as lasing devices [5,6] were demonstrated in this material. However, at high injection currents or high pump powers, degeneration of the spontaneous and stimulated emission from such devices is caused by strain relaxation and interdiffusion [7]. Because of these effects, group III nitrides and their alloys are superior due to structural and mechanical stability [8–11], but ZnSe and related materials still have the advantage of the availability of cheap GaAs substrates with small lattice mismatch to ZnSe. Consequently, typical heterostructures based on this material provide excellent crystal quality (e.g., low defect density).

The latter are required for several modern device applications of current research interest, such as low-threshold lasers based on micro- and nanocavity implementations [12], optically pumped single-photon sources [13–16], or single quantum dot photodiodes [17]. Such devices allow for operation with small enough pump powers or injection currents to maintain structural integrity of ZnSe based heterostructures. Presently of particular interest in this context are II-VI quantum wells (QWs) that are δ doped with shallow impurities: Stimulated emission from microdisk cavities based on fluorine doped ZnSe/(Zn,Mg)Se QWs was achieved and optically pump powers of about 15 W cm^{-2} were sufficient to initiate lasing in the blue spectral range [18,19].

Single photon emission from nitrogen acceptor centers in ZnSe was first shown in Ref. [20]. More recently, indistinguishable single photon emission [21] and post-selection of entangled photon pairs [22] from two independent nanodevices based on single fluorine donors in ZnSe/(Zn,Mg)Se QW nanostructures was demonstrated. Similar structures were also used to generate optically controllable spin qubits with fluorine donors in ZnSe QWs [23,24]. However, the spectral bandwidth of the single-photon emission, lasing, or qubit applications from the above mentioned examples is limited to the blue spectral range, mainly determined by the properties of the ZnSe QW. Ternary alloyed (Zn,Cd)Se QWs enable the access to the green spectral range and would allow the realization of integrated-optical implementations [e.g., lower absorption coefficients in the ZnSe and (Zn,Mg)Se] based on waveguides. However, alloy fluctuations and increasing lattice mismatch between ZnSe and (Zn,Cd)Se are drawbacks of a higher cadmium content so that optimization of such quantum structures remains challenging.

Alternatively, alloy fluctuations are significantly reduced for pure binary CdSe QWs enclosed in ZnSe barriers, but then the large lattice mismatch of CdSe to ZnSe and to the commercial available GaAs substrates limits the critical thickness to about 2 ML. For a CdSe coverage between 2 and 3 ML usually QDs are formed via the Stranski-Krastanov process [25]. Further increase of the CdSe thickness above a coverage of 3.1 ML leads to structural disorder due to starting of plastic lattice relaxation [25]. Similar behavior was also shown for CdTe/ZnTe epilayers, but in this material system the threshold of plastic lattice relaxation was found to be substantially higher (about 5 ML) [26] although the relative lattice mismatch of CdSe/ZnSe and CdTe/ZnTe are nearly equal. However, in both materials the plastic relaxation leads to complete vanishing of the photoluminescence (PL) efficiency [26–28]. Many efforts were performed to investigate and improve the ZnSe/CdSe QW interface and besides structural disorder, interface roughness and in thin QWs also interface alloying between ZnSe and CdSe are considered as the limiting factors [29,30]. Therefore, so far only poor results have been achieved towards high quantum efficiency of CdSe/ZnSe QWs at room temperature and low inhomogeneous broadening of the PL emission at liquid helium (LHe) temperature.

*apawlis@mail.upb.de

 ©2015 American Physical Society

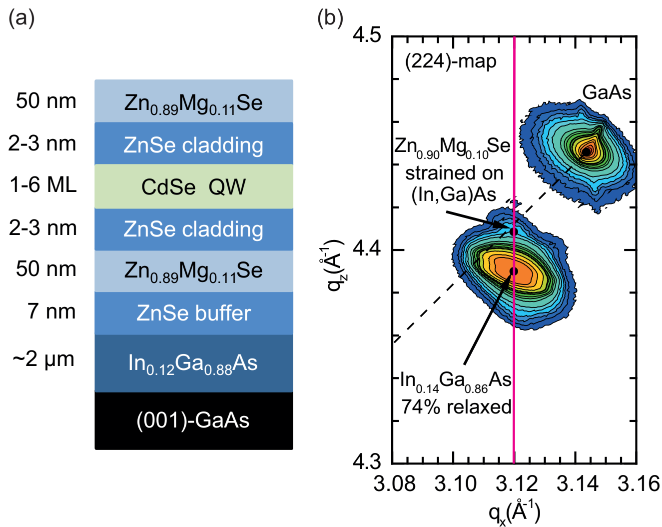

FIG. 1. (Color online) (a) Exemplary sample structure of the (Zn,Mg)Se/ZnSe/CdSe QWs investigated here. The samples are grown on an (In,Ga)As layer of about 2 μm thickness on top of GaAs substrates. The (In,Ga)As is nearly fully relaxed and provides a substrate with smaller misfit to CdSe. (b) Reciprocal space map close to the (224) reflex of one of the studied samples (sample B). The $Zn_{0.9}Mg_{0.1}Se$ reflex is nearly on top of the (In,Ga)As reflex, which indicates that it is nearly lattice matched to the (In,Ga)As.

II. EXPERIMENTAL DETAILS

Here we focus on the structural and optical properties of heterostructures, where binary CdSe QWs are embedded in ZnSe cladding layers and (Zn,Mg)Se barriers. Furthermore, these heterostructures were grown on thick (In,Ga)As templates, which provide a larger lattice parameter and therefore reduced lattice mismatch to the CdSe as a function of an increasing indium concentration. The magnesium concentration of 10%–12% was especially chosen such that the (Zn,Mg)Se barriers are most likely lattice matched to the (In,Ga)As. Hence the major fraction of the strain in the structure is only accumulated in the CdSe/ZnSe QW region. In the latter case the lattice parameter of ZnSe is substantially smaller, respectively, while that of the CdSe is still considerably larger when compared to the lattice parameter of the (In,Ga)As. Consequently, the ZnSe cladding layers are tensile strained while the CdSe QW is compressively strained in the investigated samples.

Figure 1(a) shows a cross-section drawing of the general sample structure of various CdSe/ZnSe/(Zn,Mg)Se QWs we studied. The samples were grown by molecular beam epitaxy (MBE) on (In,Ga)As templates with 12%–14% indium concentration. The (In,Ga)As templates have a thickness of about 2 μm and were grown on commercial available GaAs substrates. Note that the indium mole fraction and the thickness of the (In,Ga)As was chosen to provide a nearly fully relaxed buffer with an in-plane lattice parameter of about 5.695 Å for the growth of the subsequent II-VI heterostructures. The MBE of the selenides was initiated with a small ZnSe buffer (7 nm) on the (In,Ga)As followed by the lower (Zn,Mg)Se barrier layer with about 50 nm thickness. The magnesium concentration of 10%–12% was chosen to enable nearly lattice-matched growth of the (Zn,Mg)Se on the (In,Ga)As. On top of the first (Zn,Mg)Se barrier a single CdSe QW was enclosed in pure ZnSe cladding layers each with a thickness of 11 ML. At last the heterostructure was terminated by another ZnMgSe barrier (50 nm). For this study we varied the thickness of the CdSe QW between 1 and 6 ML. As we will show later on, this variation is sufficient to cover nearly the whole visible spectral range.

The lattice configuration of a typical heterostructure (sample B) is characterized by the asymmetric (224)-reflex reciprocal space map in Fig. 1(b). The (In,Ga)As has an indium mole fraction of about 0.14 ± 0.01 and is about 74% relaxed relative to the GaAs substrate (e.g., the dashed line corresponds to fully relaxed cubic lattice in the reciprocal space). In contrast, the (Zn,Mg)Se reflex is pseudomorphically strained on the (In,Ga)As and only visible as a small shoulder close to the (In,Ga)As reflex, which indicates nearly lattice-matched growth of the (Zn,Mg)Se layers. The estimated magnesium concentration is about $10 \pm 1\%$.

All photoluminescence measurements were performed in a confocal μ-PL setup with a spatial resolution of about 2 μm. The luminescence was dispersed in a 500 mm spectrometer (spectral resolution of about 300 μeV) and detected with a LN_2 cooled silicon based CCD array. For excitation we used a constant wave semiconductor laser at $\lambda = 378$ nm. The power was varied between 50 nW and 50 μW and focused down to a spot size of about 2 μm diameter.

A complete list of the important growth parameters of the sample series for this study is summarized in Table I. The magnesium and indium concentrations were derived from reciprocal space maps around the (224) reflex as measured by high resolution x-ray diffraction (HRXRD) [see also Fig. 1(b)]. The widths of the ZnSe cladding layers and the CdSe QWs were calculated from time-resolved RHEED-intensity oscillation measurements. The special feature of the samples in Table I is that the ZnSe cladding layers are substantially tensile strained, while the CdSe QWs remain strongly compressively strained on the (In,Ga)As templates. Here we consider that the main amount of strain energy is accumulated in the central ZnSe/CdSe/ZnSe region of the samples because the (Zn,Mg)Se barriers are nearly lattice matched to the (In,Ga)As and the initial small ZnSe seeding layer is far away from the quantum region of the structure. Such special layer sequence composed of a stack of alternating tensile

TABLE I. Overview of the characteristic features of the (Zn,Mg)Se/ZnSe/CdSe QW heterostructures of this study.

Sample	d(ZnSe) cladding (ML)	d(CdSe) QW (ML)	Mg content (%)	In content (%)
A (2101)	0	1.6	8	14
B (2103)	7	1.6	10	14
C (2126)	11	1.0	12	13
D (2125)	11	1.8	11	12
E (2140)	11	2.0	12	12
F (2143)	11	2.5	12	12
G (2120)	11	3.1	11	12
H (2121)	11	3.9	12	13
I (2122)	11	4.7	11	12
J (2135)	11	5.6	11	12

and compressively strained components may lead to strain compensation effects [31]: For example, in Refs. [32,33] μ-Raman spectroscopy was performed in a similar system [e.g., free-standing (Zn,Mg)Se/ZnSe QWs with a lattice parameter $a_{\text{ZnMgSe}} > a_{\text{ZnSe}}$]. The shift of the LO-phonon lines of (Zn,Mg)Se and ZnSe revealed that such a layer system minimizes its elastic energy density by the relaxation to an average lattice parameter $a_{\text{eq.}}$ with the condition $a_{\text{ZnMgSe}} > a_{\text{eq.}} > a_{\text{ZnSe}}$. The measurements confirmed that (Zn,Mg)Se was compressively strained and ZnSe tensile strained relative to the average lattice parameter ($a_{\text{eq.}}$). The latter depends on the overall volume ratio between the participating layer materials and can be estimated by the calculation of a weighted average based on the thickness of the corresponding layers. Including this strain minimization effect of alternating layer systems into our model calculations presented in Sec. IV, we describe the whole ZnSe/CdSe/ZnSe sequence as a combined system with a quasicubic arrangement with $a_{\text{eq.}}$ as the equilibrium lattice parameter [31]. Note that this description is an approximation which in our opinion is valid in the scope of this article, since *ab initio* calculations of the real local strain distribution in the layer system would require us to consider a supercell including the coordinates of about one million atoms, which might exceed practicable computing resources.

III. RESULTS AND DISCUSSION

Figure 2 shows the impact of the ZnSe cladding layers on the PL properties of 1.6 ML thick CdSe QWs. In case of sample A the CdSe was directly terminated with (Zn,Mg)Se barriers while for sample B about 7 ML thick ZnSe cladding layers were introduced in between. The corresponding low-temperature PL spectra of the samples are presented in Fig. 2(a) and were fitted with Gaussian curves to estimate the spectral full-width-at-half-maximum (FWHM). The inhomogeneous linewidth of the PL of sample B is reduced by about 40% relative to that of sample A. We attribute this remarkable effect not only to the suppression of alloy fluctuations due to the binary/binary QW interfaces in sample B but also to a significant strain compensation in the structure. The redshift of the PL peak maximum of sample B stems from the reduced confinement energy of the ZnSe versus the (Zn,Mg)Se. The spectra at ambient conditions are shown in Fig. 2(b) and denote the same trend but a smaller reduction of the FWHM spectral linewidth. For a moderate excitation power of about 400 W cm^{-2} we measured a room-temperature PL intensity of about 2.6×10^3 counts per seconds (cps) in sample A while at the same conditions the intensity of sample B was nearly a factor of 10 higher. The strong increase of intensity and the reduction of the FWHM linewidth shown in Fig. 2 reflects the improvement of the optical properties of CdSe QWs due to the embedding into ZnSe cladding layers.

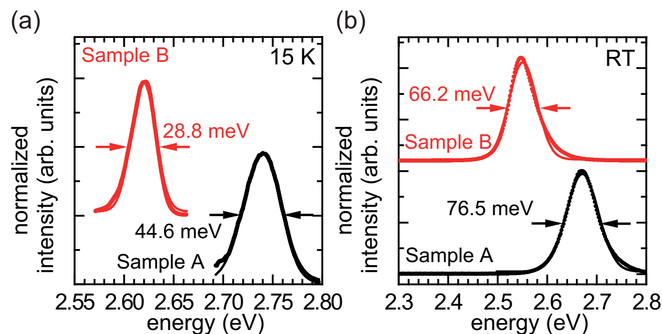

FIG. 2. (Color online) Normalized PL spectra at (a) about 15 K and (b) at room temperature of sample A (black) and sample B [red (gray)], both with 1.6 ML CdSe QW thickness and similar magnesium concentration. For sample A the CdSe QW was enclosed only in (Zn,Mg)Se barriers, while for sample B ZnSe cladding layers were introduced between the (Zn,Mg)Se and CdSe. The latter denotes a significantly reduced inhomogeneous linewidth of the PL emission in (a) and (b).

In most of the previous investigations of CdSe QWs in ZnSe or (Zn,Mg)Se barriers [27–30] a drastic reduction of the PL intensity and increase of the spectral linewidth was reported for a thickness exceeding 3 ML. This limit was attributed to the generation of misfit dislocations upon lattice relaxation of strained CdSe on ZnSe or GaAs (lattice mismatch about 6.7%). Although the (In,Ga)As templates used for this study provide a slightly reduced lattice mismatch of about 6.3% no significant increase of the critical thickness of the CdSe is expected [34]. However, we observed surprisingly efficient PL emission for CdSe QWs with a thickness close to 6 ML.

Figure 3 shows the PL spectra at room temperature (left side) and at 15 K (right side) measured from the series (B–J) of CdSe QWs (1.0–5.6 ML width). The peaks were fitted by Gaussian curves as indicated by the red (gray) lines. The room temperature emission [Fig. 3(a)] is of high relevance for possible device applications. The spectra denote a linewidth which is between 40 and 60 meV and nearly independent of the QW thickness up to 3.9 ML. Though a significant increase of the linewidth is observed for a CdSe QW thickness $\geqslant$3.9 ML.

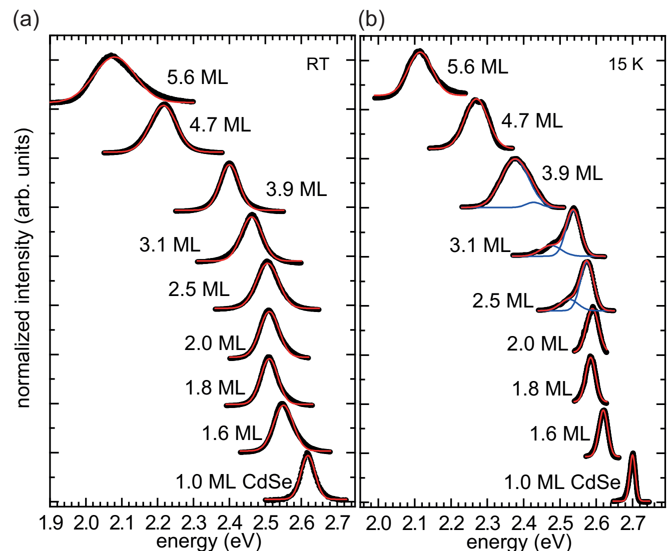

FIG. 3. (Color online) Normalized PL spectra at room temperature (a) and at about 15 K (b) of a series (B–J) of CdSe QWs with 1.0–5.6 ML thickness enclosed in ZnSe cladding layers. The overall covered spectral range is about 600 meV and corresponds to an emission wavelength range of 470–600 nm. The red (gray) and blue (dark gray) curves are Gaussian fits.

For a moderate excitation power of about 160 W cm^{-2}, we measured PL intensities ranging from 3×10^2 to 3×10^3 cps in the case of most of the samples. Significant reduction of the room temperature emission only occurs in sample C (150 cps) with the smallest QW and in sample J (31 cps) with the largest QW. Note that by our variation of the CdSe QW width between 1 and 6 ML we were able to tune the emission energy in a range of about 600 meV from the blue to the red visible spectrum.

For the low temperature spectra in Fig. 3(b) we used an extremely low excitation power density of roughly 2 W cm^{-2} and still obtained significant PL emission of several hundred cps. For the CdSe QW with 1.0 ML thickness (sample B) we obtained a peak emission energy of about 2.700 eV and a FWHM spectral width of 18 meV at low temperature, which is in good agreement with previous studies of a similar sample performed in Ref. [27]. With increasing QW width up to two ML the linewidth of the emission is also slightly increased and the emission energy is redshifted as well. In case of the spectra measured from the 2.5, 3.1, and 3.9 ML thick CdSe QWs (samples F–H) we resolved two peaks contributing to the overall luminescence. These spectra were independently fitted with two Gaussian subpeaks [blue (dark gray) curves]. We attribute the two peaks to contributions of heavy-hole (at lower energy) and light-hole (at higher energy) related emission, which we will explain by the induced strain compensation (see details in Sec. IV). The unusual intensity distribution, indicating much higher luminescence intensity of the higher-energy peaks (light hole) in the samples with 2.5 and 3.1 ML CdSe could be due a phonon mediated internal coupling between the heavy-hole and light-hole band of CdSe, since their energy splitting is roughly equal to the longitudinal-optical (LO) phonon energy of CdSe. We performed exemplary temperature dependent PL measurements of the 2.5 ML sample (not shown here) and observed a vanishing of the lower energy peak with increasing temperature and the Arrhenius plot of the relative integral intensity of the lower and higher energy peaks (not shown here) indicates that the relevant process has an activation energy of about 19 meV. The latter is in the same order as the heavy-hole/light-hole splitting in CdSe we calculated via model B (10 meV). However, possible coupling between the hole states is not investigated here and requires further experiments, which might be central aspect of a different paper. Note that in case of the 3.9 ML CdSe QW sample we observed a substantially broader linewidth of the emission than in the other samples which might be due to less optimized growth conditions with higher interface roughness. Moreover, the higher energy peak of the two Gaussion subpeaks is nearly vanishing and a strong redshift of the central energy of the luminescence is observed when compared to that of the 3.1 ML thick sample. This difference of the shape of the emission peaks suggest a vanishing of the above mentioned internal coupling between the heavy-hole (HH) and light-hole (LH) transitions. Generally, if the CdSe QW thickness exceeds 3.1 ML in the samples, the peak splitting is not resolved anymore but also the linewidth of the emission is significantly increased. Unlikely, the latter could be a consequence of lattice relaxation. If this would be the case in our samples, however, it does not lead to the observed quenching of the PL intensity reported in the previous studies [27,28]. For a moderate excitation power of about 160 W cm^{-2}, we measured low temperature PL intensities ranging from 1×10^4 to 1×10^5 cps in the case of all of the samples. Note that at this power density significant PL emission is observed from the CdSe QWs with 4.7 ML (intensity 1.4×10^5 cps) and 5.6 ML (intensity 1.9×10^4 cps) width, although the thickness of these QWs is far above the critical thickness.

IV. MODEL AND CALCULATIONS

For providing a detailed interpretation of the observed low temperature PL spectra in Fig. 3(b) we modeled the band structure and transition energies close to the Γ point of the heterostructures by using the *nextnano*^{3} simulation software [35]. The calculations are based on solving the Schrödinger equation, using the effective-mass model and considering the strain state (Pikus-Bir Hamiltonian) of the layers. The corresponding pseudomorphic lattice deformation is given by the Poisson ratios of the materials and leads to a hydrostatic and uniaxial pressure. According to the Pikus-Bir Hamiltonian the hydrostatic component changes the band gap at the Γ point while the uniaxial pressure splits the valence bands into the HH and LH branch. The general parameters we used for modeling the ZnSe and (Zn,Mg)Se are the same as in Ref. [36] and the ternary material was linearly interpolated (Vegard's law).

For the CdSe QWs we assumed cubic crystal structure and the main material parameters as summarized in Table II together with a valence band offset of 20% to ZnSe [44]. We assumed excitonic transitions in the CdSe QWs, considered the exciton binding energy and calculated the average strain energy density across the ZnSe/CdSe/ZnSe layer system with the *nextnano*^{3} software. In the following we discuss two independent model approaches (termed models A and B) for the calculations of the low temperature excitonic transitions in the ZnSe/CdSe/ZnSe quantum region as a function of the CdSe well width. Note that due to the complete parameter sets in Ref. [36] and Table II as well as the experimental information (magnesium concentration, ZnSe thickness, and CdSe QW width) no free parameter is remaining for any fitting of the calculated data with the measured peak energies.

In our first approach (model A) we considered the strain state in each of the layers separately as given by the relative lattice mismatch between the cubic lattice of the layer materials and the in-plane lattice parameter of the (In,Ga)As template (about 5.695 Å). This leads to a substantial tensile strain in the ZnSe and enormous compressive strain in the CdSe, so that the

TABLE II. Material parameters of CdSe that we used for our calculation.

Parameter	Value	Reference
m_e^* (units of m_0)	0.12	[37]
m_{hh}^* (units of m_0)	0.9	[37]
m_{lh}^* (units of m_0)	0.18	[37]
E_g (eV)	1.9	[38]
a_0 (nm)	0.6052	[39]
c_{11} (GPa)	74.6	[40]
c_{12} (GPa)	46.1	[40]
a (eV)	−2.3	[41,42]
b (eV)	−0.8	[43]

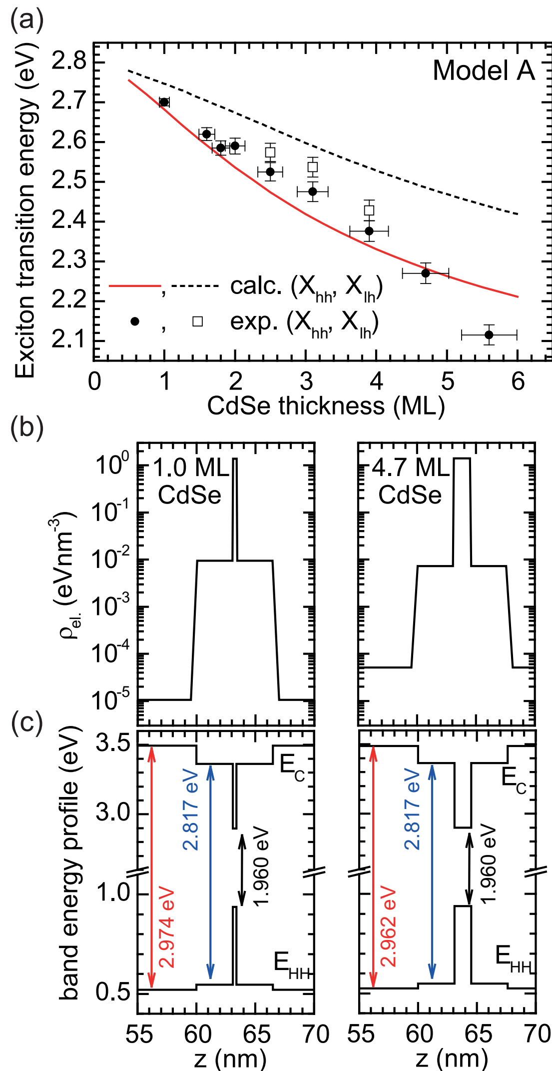

FIG. 4. (Color online) Overview of the results of the band structure simulation performed with model A and experimental data. (a) Transition energies involving the electron/HH ground states [red (gray line)] as well as electron/LH ground states (dashed line) versus CdSe QW thickness. The experimental PL peak energies (dots and open squares) were extracted from Fig. 3(a). (b) Exemplary calculations of the strain energy density along the cross section (i.e., in growth direction z) of the quantum region for samples C (left) and I (right). (c) Corresponding band structure and confinement potentials for electrons and heavy holes at the Γ point of samples C and I.

lowest-energy excitonic transition is formed by electron and heavy-hole confined states. Figure 4(a) shows the results of the simulations based on model A. The black dots are the experimental results (lowest energy peak, HH related) as extracted from the Gauss fits of the PL spectra in Fig. 3(a) versus the thickness of the CdSe QWs. The open squares correspond to the energy of the second transition (higher energy, LH related) we extracted from the spectra of samples F, G, and H (with 2.5, 3.1, and 3.9 ML QW). The thickness of the QWs was calculated from the growth rate, which we extracted several times from RHEED oscillation measurements during the deposition of the CdSe. The error bars reflect the variation of the emission energy resulting from the estimated uncertainty (about 7%) of the CdSe growth rate. The red (gray) line depicts the calculated lowest transition composed of electron and heavy-hole versus CdSe well width for a set of fixed growth parameters (e.g., 11% magnesium concentration, 11 ML thick ZnSe cladding layers, and an in-plane (In,Ga)As lattice parameter of 5.695 Å). The dashed line shows the lowest transition composed of electron and light-hole with the same parameters. As evident from Fig. 4(a) substantial deviation between the measured peak energies and calculated results is observed. Unlikely, this deviation could be explained by interdiffusion between ZnSe and CdSe: Such effect was only predicted in Ref. [29] in case of CdSe QWs with submonolayer thickness. Moreover, interdiffusion would be limited to a region within 1–2 ML close to the CdSe/ZnSe interface so that one would expect a reduced impact of interdiffusion with increasing CdSe well width, but this trend is not observed in Fig. 4(a). We attribute the deviation between the measured peak positions and the calculated ground state transition to the fact that the alternating tensile and compressive strain in the ZnSe/CdSe/ZnSe cannot be considered independently for each of the layers (see model B).

Exemplary details of the simulations are shown in Figs. 4(b) and 4(c) in case of sample C (left side) and sample I (right side) which contain a 1.0 and a 4.7 ML thick CdSe QW, respectively. The plots in Fig. 4(b) illustrate the strain energy density $\rho_{el.}$ along the cross section of the heterostructures (i.e., in growth direction z) zoomed in close to the relevant quantum region. The (Zn,Mg)Se barriers are nearly lattice matched to the (In,Ga)As ($\rho_{el.} < 10^{-4}$ eV nm^{-3}), while that of the ZnSe cladding layers is about two orders of magnitude higher. The enormous compressive strain in the CdSe QW leads to strain energy densities exceeding 1 eV nm^{-3}. The plots in Fig. 4(c) show the corresponding band energy profile close to the Γ point of samples C and I on the same length scale. The red (gray) arrow indicates the band gap of the (Zn,Mg)Se which is slightly different due to a small variation of the magnesium concentration between the two samples. The band gaps of the ZnSe cladding and the CdSe QW are identical within the estimated numerical error of (±1 meV) of the simulation.

In our second improved approach (model B) we tried to implement the previously mentioned strain compensation effect between the alternating tensile and compressive strain in the ZnSe/CdSe/ZnSe layer system based on the following two assumptions: (1) The calculations of the ground-state wave functions of electron and heavy-hole with model A confirm a complete distribution of the wave functions over the whole ZnSe/CdSe/ZnSe layer system for a CdSe QW thickness up to 4.7 ML. Consequently, we assume that the confined excitons "see" an average lattice mismatch, which due to the alternating strain directions in the subsystem is smaller than that of the individual layers. Within our computational possibilities we considered the strain situation by an equilibrium cubic lattice parameter $a_{eq.}$ in the three-layer system. Such an approach was first introduced by Lentz *et al.* in 1989 to describe the characteristics of CdTe/CdZnTe superlattices [31]. The equilibrium lattice parameter of the ZnSe/CdSe/ZnSe subsystem is calculated similar as in Refs. [32,33] by a weighted average

based on the thickness ratio of the ZnSe and CdSe layers

$$a_{\mathrm{eq.}} = \frac{d_{\mathrm{ZnSe}}}{d_{\mathrm{ZnSe}} + d_{\mathrm{CdSe}}} * a_{\mathrm{ZnSe}} + \frac{d_{\mathrm{CdSe}}}{d_{\mathrm{ZnSe}} + d_{\mathrm{CdSe}}} * a_{\mathrm{CdSe}}. \quad (1)$$

Hence, we suppose that the ZnSe/CdSe/ZnSe layer system might be described as a free standing state with the equilibrium lattice parameter $a_{\mathrm{eq.}}$ given above. (2) The (In,Ga)As templates provide a lateral lattice parameter of about 5.695 Å and the HRXRD measurements indicate that the whole II-VI heterostructure is pseudomorphically strained on the (In,Ga)As. Consequently, we assumed that the remaining strain in the ZnSe/CdSe/ZnSe layer system is characterized by the lattice mismatch between $a_{\mathrm{eq.}}$ and the lateral (In,Ga)As lattice parameter. Using this lattice mismatch in model B, we followed the Pikus-Bir formalism to calculate the change of the band gap due to the hydrostatic and uniaxial strain. Effectively this leads to a smaller HH/LH splitting of the band structure at the Γ point compared to that of model A. Note that we did not introduce a weighted average for the Poisson ratios, since the latter are nearly equal for CdSe ($p_{\mathrm{CdSe}} = 0.618$) and ZnSe ($p_{\mathrm{ZnSe}} = 0.603$).

Figure 5 illustrates the results of the calculations according to model B. The diagrams are arranged in the same layout as those in Fig. 4. The good agreement between the experimental data (dots) and the calculated electron/HH ground state transition in Fig. 5(a) is obviously visible. Moreover, due to the reduced strain in the structure, the energy splitting between the HH and LH related transitions is reduced so that also the experimentally observed LH related peaks (open squares) are matching the calculated transitions (dashed line). The inset in Fig. 5(a) shows the equilibrium lattice parameter as the function of the CdSe well width. We found a significant increase of $a_{\mathrm{eq.}}$ as we kept the ZnSe cladding layer thickness constant for samples C–J. Therefore, the weighted average is continuously shifted to the CdSe lattice parameter for a larger QW size. Consequently, more and more strain is introduced in the ZnSe/CdSe/ZnSe quantum region due to the increasing lattice mismatch to the (In,Ga)As templates. This effect is also evident in the strain energy densities in Fig. 5(b), which change from $\rho_{\mathrm{el.}} \approx 1\times10^{-3}$ eV nm^{-3} for sample C to $\rho_{\mathrm{el.}} \approx 3\times10^{-2}$ eV nm^{-3} for sample I, respectively.

In the case of sample J (5.6 ML CdSe) the theoretical transition energy is significantly blueshifted relative to the experimental result. Indeed, this particular sample is not appropriately described: The total thickness of the ZnSe/CdSe/ZnSe layer system is about 8 nm in sample J (5.6 ML CdSe) and the relative lattice mismatch between $a_{\mathrm{eq.}}$ and the (In,Ga)As substrate is about 1.0%. According to the model in Ref. [34] this leads to a critical thickness $h_c \approx 7$ nm so that sample J might be already relaxed. This can also explain the reduced quantum efficiency and increased linewidth of the PL (see also Fig. 3). In contrast, sample I (4.7 ML CdSe) has an overall thickness of the ZnSe/CdSe/ZnSe region of about 7 nm and the corresponding $a_{\mathrm{eq.}}$ leads to a lattice mismatch of 0.8%, for which the critical thickness is $h_c \approx 10$ nm, so that this sample (and also samples B–H) can be considered as pseudomorphically strained on the (In,Ga)As templates. In particular, samples I and J indicate that our model of the effective strain and an equilibrium lattice parameter in the ZnSe/CdSe/ZnSe stack forms an adequate basis, which

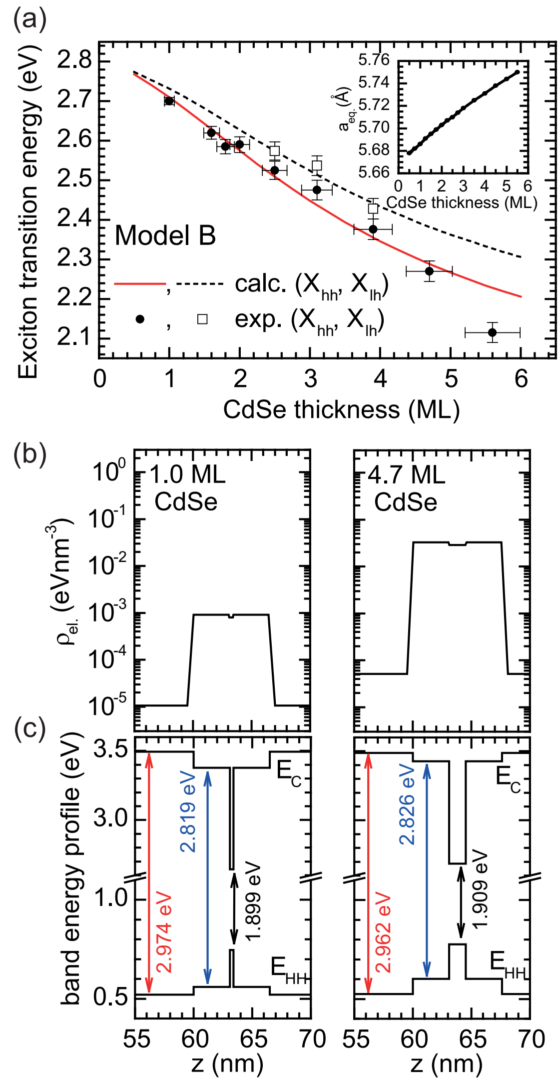

FIG. 5. (Color online) Overview of the results of the band structure simulation performed with model B and experimental data. (a) Transition energies involving the electron/HH ground states [red (gray line)] as well as electron/LH ground states (dashed line) versus CdSe QW thickness and the experimental PL peak energies (dots and open squares). The inset shows the calculated lattice parameter $a_{\mathrm{eq.}}$ versus CdSe well width. (b) Exemplary calculations of the strain energy density along the cross section of the quantum region for samples C (left) and I (right). (c) Corresponding band structure and confinement potentials for electrons and heavy holes at the Γ point of samples C and I.

also allows us to understand the observed features in the framework of strain relaxation and critical thickness of the samples.

The PL spectra of samples F–H indicate that two independent peaks contribute to the PL, for which we assumed that the lower energy peak stems from a heavy-hole exciton and the higher energy peak corresponds to a light-hole exciton. Our calculations with model B verify that for those three samples the energy splitting between the HH and LH band of the CdSe is between 13 and 33 meV, which is close to typical phonon energies in bulk CdSe [2] (about 27 meV). The presence of the

LH related transition in those specific samples could be due to phonon coupling. However, no contribution of the LH related transitions is observed in the spectra of samples B–E as well as samples I and J. According to model B, the HH/LH splitting is much smaller than the LO phonon energy in CdSe and the linewidth of the observed PL peaks of samples B–E. In case of samples I and J the HH/LH splitting is much larger than the phonon energy. This might be one reason why the HH and LH related transitions are only prominently visible in the samples F–H. Further studies are required to investigate this effect, but those are beyond the scope of this publication.

Figure 5(b) illustrates the strain energy density and the band gap profile for sample C (left) and sample I (right) as calculated based on model B. Over the whole ZnSe/CdSe/ZnSe quantum region the average strain energy density is constant due to the implemented strain compensation effect with resulting $a_{eq.}$ lattice parameter. The negligible small variation between the strain energy density of ZnSe and CdSe results from slightly different Poisson ratios in the two materials. Figure 5(c) shows the band energy profile along the growth axis of the layers on the same length scale as the strain distribution above. Since the $a_{eq.}$ is always larger than the (In,Ga)As lattice parameter for a QW thickness exceeding 0.5 ML [see also inset in Fig. 5(a)], a net compressive strain across the whole ZnSe/CdSe/ZnSe region is induced. For the ZnSe cladding layers this leads to an electron/HH band gap, which increases with larger CdSe well width (from 2.819 eV in sample C to 2.826 eV in sample I). The situation is similar in the CdSe where the electron/HH band gap is rising from 1.899 to 1.909 eV. This results in a blueshift of the electron/HH and a redshift of the electron/LH transitions and leads to the significantly improved matching of the observed and calculated transition energies in model B.

V. CONCLUSIONS

We demonstrate efficient low- and room-temperature PL emission and spectral tuning of epitaxially grown ZnSe/CdSe based quantum well structures over the whole visible spectrum covering a wavelength range between 600 and 470 nm. The key element of the observed high quantum efficiency and large tuning range is the implementation of a strain engineering technique, which allows us to overcome the limiting lattice relaxation of CdSe on ZnSe. The latter is normally induced by the large lattice mismatch of nearly 7% between the two materials. Previous studies indicated that plastic relaxation of CdSe on ZnSe occurs already at a coverage exceeding 3.1 ML and leads to immediate lattice relaxation by the formation of lattice defects. As a consequence complete quenching of the photoluminescence efficiency at low and also at room temperature was observed.

In contrast, our approach enables the deposition of CdSe quantum films with a thickness between 1 and 6 ML via a balanced epitaxy process where thickness and strain between alternating tensile (ZnSe) and compressively strained (CdSe) layers was adjusted to minimize the strain. Such ZnSe/CdSe quantum wells provide excellent optical properties within the above mentioned large spectral tuning range. Although previous studies also demonstrated the formation of CdSe quantum dots for a coverage of 2.0–3.1 ML the small linewidth of the observed PL emission suggests that quantum dot formation is suppressed and the PL emission originates from a pure QW system.

We modeled the observed experimental features with two different models (models A and B). The first model is based on an individually separately treatment of each of the layers and the second model considered the ZnSe/CdSe/ZnSe layer system conjointly. The good agreement between the experimental findings and calculations of the transition energies of the ZnSe/CdSe QWs with model B provides a firm ground for our proposed strain compensation effect that can be present in such an alternating system of tensile and compressively strained epitaxial layers.

ACKNOWLEDGMENTS

This work was funded by the Volkswagen Foundation (Project 88360) and the Deutsche Forschungsgemeinschaft (Project LI668/8-1). A.P. would further like to thank Dr. S. Birner (nextnano GmbH) for fruitful discussions and support on the *nextnano*^{3} simulation software. D.R. greatfully acknowledges support by the DFG via TRR-142 and the BMBF Q.com-H 16KIS0114. A.L. and A.D.W. acknowledge gratefully support of Mercur Pr-2013-0001, BMBF Q.com-H 16KIS0109, and the DFH/UFA CDFA-05-06.

[1] J. Puls, M. Rabe, A. Siarkos, and F. Henneberger, Phys. Rev. B **57**, 14749 (1998).
[2] F. Gindele, U. Woggon, W. Langbein, J. M. Hvam, K. Leonardi, D. Hommel, and H. Selke, Phys. Rev. B **60**, 8773 (1999).
[3] J. I. Nishizawa, K. Itoh, Y. Okuno, and F. Sakurai, J. Appl. Phys. **57**, 2210 (1985).
[4] D. Eason, Z. Yu, W. Hughes, W. Roland, C. Boney, J. Cook, J. Schetzina, G. Cantwell, and W. Harsch, Appl. Phys. Lett. **66**, 115 (1995).
[5] H. Okuyama, T. Miyajima, Y. Morinaga, F. Hiei, M. Ozawa, and K. Akimoto, Electron. Lett. **28**, 1798 (1992).
[6] F. Nakanishi, H. Doi, N. Okuda, T. Matsuoka, K. Katayama, A. Saegusa, H. Matsubara, T. Yamada, T. Uemura, M. Irikura *et al.*, Electron. Lett. **34**, 496 (1998).
[7] M. Hovinen, J. Ding, A. Salokatve, A. V. Nurmikko, G. C. Hua, D. C. Grillo, L. He, J. Han, M. Ringle, and R. L. Gunshor, J. Appl. Phys. **77**, 4150 (1995).
[8] T. Frey, D. As, M. Bartels, A. Pawlis, K. Lischka, A. Tabata, J. Fernandez, M. Silva, J. Leite, C. Haug *et al.*, J. Appl. Phys. **89**, 2631 (2001).
[9] S. Li, J. Schörmann, A. Pawlis, D. J. As, and K. Lischka, Microelectron. J. **36**, 963 (2005).
[10] A. Tamboli, E. Haberer, R. Sharma, K. Lee, S. Nakamura, and E. Hu, Nat. Photon. **1**, 61 (2007).
[11] M. Bürger, G. Callsen, T. Kure, A. Hoffmann, A. Pawlis, D. Reuter, and D. J. As, Appl. Phys. Lett. **103**, 021107 (2013).
[12] M. Hovinen, J. Ding, A. V. Nurmikko, D. C. Grillo, J. Han, L. He, and R. L. Gunshor, Appl. Phys. Lett. **63**, 3128 (1993).

[13] K. Sebald, P. Michler, T. Passow, D. Hommel, G. Bacher, and A. Forchel, Appl. Phys. Lett. **81**, 2920 (2002).
[14] K. De Greve, S. M. Clark, D. Sleiter, K. Sanaka, T. D. Ladd, M. Panfilova, A. Pawlis, K. Lischka, and Y. Yamamoto, Appl. Phys. Lett. **97**, 241913 (2010).
[15] A. Tribu, G. Sallen, T. Aichele, R. André, J.-P. Poizat, C. Bougerol, S. Tatarenko, and K. Kheng, Nano Lett. **8**, 4326 (2008).
[16] S. Bounouar, M. Elouneg-Jamroz, M. Hertog, C. Morchutt, E. Bellet-Amalric, R. André, C. Bougerol, Y. Genuist, J.-P. Poizat, S. Tatarenko *et al.*, Nano Lett. **12**, 2977 (2012).
[17] M. Panfilova, S. Michaelis De Vasconcellos, A. Pawlis, K. Lischka, and A. Zrenner, Physica E **42**, 2521 (2010).
[18] A. Pawlis, M. Panfilova, D. J. As, K. Lischka, K. Sanaka, T. D. Ladd, and Y. Yamamoto, Phys. Rev. B **77**, 153304 (2008).
[19] A. Pawlis, M. Panfilova, K. Sanaka, T. D. Ladd, D. J. As, K. Lischka, and Y. Yamamoto, Microelectron. J. **40**, 256 (2009).
[20] S. Strauf, P. Michler, M. Klude, D. Hommel, G. Bacher, and A. Forchel, Phys. Rev. Lett. **89**, 177403 (2002).
[21] K. Sanaka, A. Pawlis, T. D. Ladd, K. Lischka, and Y. Yamamoto, Phys. Rev. Lett. **103**, 053601 (2009).
[22] K. Sanaka, A. Pawlis, T. D. Ladd, D. J. Sleiter, K. Lischka, and Y. Yamamoto, Nano Lett. **12**, 4611 (2012).
[23] Y. M. Kim, D. Sleiter, K. Sanaka, Y. Yamamoto, J. Meijer, K. Lischka, and A. Pawlis, Phys. Rev. B **85**, 085302 (2012).
[24] D. J. Sleiter, K. Sanaka, Y. M. Kim, K. Lischka, A. Pawlis, and Y. Yamamoto, Nano Lett. **13**, 116 (2013).
[25] D. Schikora, S. Schwedhelm, D. As, K. Lischka, D. Litvinov, A. Rosenauer, D. Gerthsen, M. Strassburg, A. Hoffmann, and D. Bimberg, Appl. Phys. Lett. **76**, 418 (2000).
[26] J. Cibert, Y. Gobil, L. Dang, S. Tatarenko, G. Feuillet, P. Jouneau, and K. Saminadayar, Appl. Phys. Lett. **56**, 292 (1990).
[27] S. Fujita, Y.-H. Wu, Y. Kawakami, and S. Fujita, J. Appl. Phys. **72**, 5233 (1992).
[28] H. Zajicek, P. Juza, E. Abramof, O. Pankratov, H. Sitter, M. Helm, G. Brunthaler, W. Faschinger, and K. Lischka, Appl. Phys. Lett. **62**, 717 (1993).
[29] Z. Zhu, H. Yoshihara, K. Takebayashi, and T. Yao, Appl. Phys. Lett. **63**, 1678 (1993).
[30] K. Leonardi, H. Heinke, K. Ohkawa, D. Hommel, H. Selke, F. Gindele, and U. Woggon, Appl. Phys. Lett. **71**, 1510 (1997).
[31] G. Lentz, A. Ponchet, N. Magnea, and H. Mariette, Appl. Phys. Lett. **55**, 2733 (1989).
[32] M. Panfilova, A. Pawlis, C. Arens, S. M. de Vasconcellos, G. Berth, K. P. Hüsch, V. Wiedemeier, A. Zrenner, and K. Lischka, Microelectron. J. **40**, 221 (2009).
[33] M. Panfilova, A. Pawlis, A. Shchekin, S. Lemeshko, and K. Lischka, Phys. Status Solidi (C) **7**, 1675 (2010).
[34] K. Pinardi, U. Jain, S. Jain, H. Maes, R. Van Overstraeten, and M. Willander, J. Appl. Phys. **83**, 4724 (1998).
[35] *The nextnano^3 software*, URL http://www.nextnano.com/index.php.
[36] A. Pawlis, T. Berstermann, C. Brüggemann, M. Bombeck, D. Dunker, D. R. Yakovlev, N. A. Gippius, K. Lischka, and M. Bayer, Phys. Rev. B **83**, 115302 (2011).
[37] Y. D. Kim, M. V. Klein, S. F. Ren, Y. C. Chang, H. Luo, N. Samarth, and J. K. Furdyna, Phys. Rev. B **49**, 7262 (1994).
[38] D. J. Stukel, R. N. Euwema, T. C. Collins, F. Herman, and R. L. Kortum, Phys. Rev. **179**, 740 (1969).
[39] W. Faschinger, P. Juza, A. Pesek, and H. Sitter, Mater. Sci. Forum **143–147**, 1617 (1994).
[40] B. Bonello and B. Fernandez, J. Phys. Chem. Solids **54**, 209 (1993).
[41] S.-H. Wei and A. Zunger, Phys. Rev. B **60**, 5404 (1999).
[42] W. Shan, W. Walukiewicz, J. W. Ager III, K. M. Yu, J. Wu, and E. E. Haller, Appl. Phys. Lett. **84**, 67 (2004).
[43] H. J. Lozykowski and V. K. Shastri, J. Appl. Phys. **69**, 3235 (1991).
[44] X. Chen, X. Hua, J. Hu, J.-M. Langlois, and W. A. Goddard, Phys. Rev. B **53**, 1377 (1996).